Sustainability in Environment
ISSN 2470-637X (Print) ISSN 2470-6388 (Online)
Vol. 11, No. 1, 2026
www.scholink.org/ojs/index.php/se

Original Paper

Spatiotemporal Mechanisms of Mountainous Urban Expansion Using Nighttime Lighting Remote Sensing—The Case of Guizhou

Bingcheng Feng[1], Anjun Lan[1], & Song Li[2*]

[1] School of Geography and Environmental Science, Guizhou Normal University, Guiyang, Guizhou 550001, China

[2] Guizhou Provincial Key Laboratory of Geographic State Monitoring of Watershed, School of Geography and Resources, Guizhou Education University, Guiyang 550018, China

[*] Corresponding Author

Received: December 23, 2025 Accepted: January 16, 2026 Online Published: February 9, 2026

doi:10.22158/se.v11n1p144 URL: http://dx.doi.org/10.22158/se.v11n1p144

Abstract

Nighttime light remote sensing has provided valuable insights into the spatiotemporal development of mountain cities across the karst area. Taking Guizhou as the study case, this study integrates DMSP/OLS and NPP/VIIRS nighttime light data from 1992 to 2022. The optimal threshold for identifying urban areas was determined through conventional data analysis. The extent of built-up areas across eight distinct periods was extracted to examine the spatiotemporal characteristics of mountain cities. The results revealed the following: The urban area of Guizhou has consistently expanded over the past three decades, with the rate and intensity of this growth following an M-shaped fluctuation pattern. The expansion rates of prefecture-level cities were categorized into four types: stable, fluctuating, breakthrough, and gradual. This urban growth predominantly followed a northeast-southwest axis. Guiyang has long served as the urban core of Guizhou, with the core shifting 42.03 km to the northeast over this period. Urban expansion exhibited three primary patterns: ring-like, linear (axial), and punctate. Notably, ring-like expansion was marked by a hollow annulus, while linear (axial) expansion mainly occurred along river valleys near smaller tributaries. The urban core of Guizhou evolved in distinct phases. Initially, Guiyang was the sole micro core, later developing into the primary core. Ultimately, a hierarchical urban structure emerged, with Guiyang as the main core, Zunyi as a secondary core, and a constellation of Kaili, Duyun, and Fuquan Cities forming peripheral micro cores. This system was characterized by Guiyang's influence over Anshun and the decentralized

growth of other cities. These findings offer important insights for urban planning and territorial development in mountain cities, such as those in Guizhou.

Keywords

night light remote sensing, urban expansion, expansion index, Guizhou

1. Introduction

Urban built-up areas, where human activities are most concentrated, are essential indicators of urbanization levels (Ouyang, Lin, Chen, Fan, Qian, & Park, 2019; He, Li, Guo, Tian, & Wang, 2019). As such, they play an important role in understanding the dynamics of urban growth (Zheng, Seto, Zhou et al., 2023). Nighttime light remote sensing has significant importance in monitoring urban expansion (Zheng, Wu, & Qian, 2019). This data has broad applications in various fields, including the estimation of socio-economic parameters and the assessment of significant events (Levin & Duke, 2012). Recent advancements in nighttime light remote sensing have offered new opportunities to explore urbanization processes in greater detail (Zhao, Zhou, Li, Cao, He, Yu, Li, Elvidge, Cheng, & Zhou, 2019; Levin, Kyba, Zhang et al., 2020). Nighttime light data are widely utilized to delineate urban built-up areas, providing valuable insights into the spatiotemporal evolution of urban environments (Huang, Luo, Wang, & Huang, 2021; Hu, Qian, Pickett et al., 2020). Consequently, a comprehensive investigation of these areas is crucial to fully understand the ongoing trends and patterns of urbanization (Ma, Li, Tong, & Liu, 2019).

Initially, DMSP/OLS data were predominantly used in early studies due to the scarcity of nighttime lighting images (Xie, Weng, & Weng, 2014; Amaral, Monteiro, Câmara et al., 2006). Since 2012, NPP/VIIRS nighttime light imagery has been the preferred data source due to its superior spatial and radiometric resolution (Ou, Liu, Li, & Li, 2015; Hillger, Seaman, Liang et al., 2014). However, its limited temporal coverage constrains its applicability for long-term urbanization studies (Bian, Li, Lei, Zhang, Nan, & Liang, 2019). A Harmonized Global Nighttime Light Dataset (1992-2018) provides globally consistent, long-term images of nighttime light emissions, enabling comprehensive analyses of urbanization, economic dynamics, and human development, with broad applications for socioeconomics, environmental science, and policy-making (Chen, Yu, Yang, Zhou, Yao, Qian, Wang, Wu, & Wu, 2021). An adjusted nighttime light dataset has been developed to extend the temporal coverage of urbanization analysis in China (Ma, Zhou, Zhou et al., 2015). Globally, the proportion of urban land increased from 0.23% to 0.53% between 1992 and 2013, with Asia experiencing the most rapid urban expansion (Zhao, Zhou, Li, Zhou, Cheng & Huang, 2020). In Russia, nighttime light growth has been uneven across federal subjects, reflecting spatial disparities in development (Yongzhen, Byambakhuu, Battsengel, Sainbuyan, & Altanbold, 2022). In China, provincial disparities in urbanization are diminishing as rapid growth in western regions increasingly converges with the more developed eastern seaboard (Li, Cao, Zhao, Jie, Liu, Chen, & Cui, 2023). Quantitative analyses of China's urbanization from 1993 to 2012 reveal a consistent outward expansion of cities from central

areas (Huang, Yang, Chen, Wu, Ren, & Liu, 2022). Nighttime light data have further facilitated detailed investigations into the spatiotemporal dynamics of urbanization across developed regions.

In China, current studies on urban expansion primarily concentrate on economically developed delta and coastal cities, often relying on single-source nighttime light data (Wang, Zheng, Han et al., 2025). Studies on underdeveloped areas remain limited, though nighttime light data has been effectively used to examine urbanization patterns in Northwest China (Ju, Dronova, Ma et al., 2017). However, the effectiveness of nighttime light remote sensing in mountain cities with complex topographies remains uncertain (Tan, 2015). Recent studies on nighttime light remote sensing have emerged as an important method for revealing the role of nighttime light data in monitoring urban expansion, assessing socioeconomic dynamics, and evaluating ecological impacts in mountainous cities. Compared to traditional remote sensing techniques, nighttime light images exhibit significant advantages in tracking urban expansion in complex terrain (Levin, Kyba, Zhang et al., 2020).

Leveraging NPP-VIIRS nighttime light remote sensing, studies can accurately identify spatial expansion patterns in mountainous cities, particularly in areas where conventional remote sensing methods struggle to capture fine-scale details (Zheng, Tang, & Wang, 2021). A strong positive correlation has been observed between nighttime light intensity and economic activity in mountainous cities (Wu, Tu, Chen et al., 2022). Moreover, the expansion of these cities often follows a "leapfrog" development pattern, heavily constrained by topographical factors (Jia, Ma, Du et al., 2020). Some studies utilizing nighttime light remote sensing highlight the ecological vulnerability of mountainous cities, underscoring the need for greater attention to sustainability concerns (Chen, Zhou, Voogt et al., 2023). Such studies highlight the regional disparities in urban growth and the challenges associated with monitoring expansion in complex terrains (Song, Li, Tao, & Liu, 2023).

2. Data and Methods

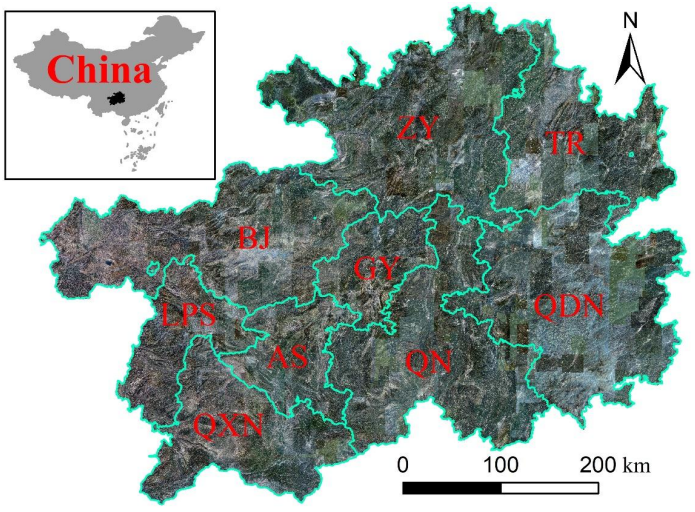

Figure 1. Study Area of Guizhou Province, China. The Abbreviations QN, QDN, and QXN are Used to Denote the Regions of Qiannan, Qiandongnan, and Qianxinan, respectively

2.1 Remotely sensed images of DMSP/OLS and NPP/VIIRS

This study employed DMSP/OLS (Xie, Weng, & Weng, 2014) and NPP/VIIRS (Wu & Wang, 2019) nighttime light images, urban built-up area data, and Guizhou administrative division vector data. Administrative division vector data were sourced from the 1:4 million database of the National Basic Geographic Information Center, while built-up area data were obtained from the Guizhou Statistical Yearbook.

The construction of a long-term sequence of nighttime light images for Guizhou from 1992-2022 included the correction and fitting of DMSP/OLS and NPP/VIIRS nighttime light images (Chen, Yu, Yang, Zhou, Yao, Qian, Wang, Wu, & Wu, 2021). The analysis of the spatiotemporal evolution of cities in Guizhou from 1992 to 2022 involved the calculation of urban expansion speed and intensity (Shen, Zhu, Cao, & Chen, 2019), the construction of the standard deviation ellipse for built-up areas, Kernel density analysis, and hotspot analysis (Bian, Li, Lei, Zhang, Nan, & Liang, 2019).

Initially, the DMSP/OLS and NPP/VIIRS images were clipped according to the research area and transformed into Albers equal-area projections. This prevented distortion from projection and aided in subsequent calculations of urban built-up areas. Then, these images were resampled to resolutions of 1 km and 500 m, respectively.

DMSP/OLS images were corrected using the constant target area method to rectify issues of instability and discontinuity in the imagery (Zhang, He, & Fan, 2017). Since a certain relationship existed between digital number (DN) in consecutive images, the images from a specific year within the constant target area were utilized to correct those from other periods (Wu, He, Peng, Li, & Zhong, 2013). Hegang, Heilongjiang, China, selected as the constant target area, experienced uniform development from 1992 to 2013. The image pixel value consistently changed, which ensured correction accuracy.

Saturation Correction and Mutual Correction. Based on the temporal variations in remote sensing data from different sources, and data saturation, phase-5 radiometrically calibrated images and their corresponding counterparts were selected for saturation correction (Hu, Chen, Cao, Chen, Cui, & Gan, 2021). Pixel values greater than 0 were grouped into the same gray matrix for linear, quadratic polynomial, logarithmic, and power regression analyses. The quadratic polynomial with the optimal fit was chosen to establish a regression model (Wang, Yao, Li, & Wu, 2017).

Radiometrically calibrated image F16_2010, along with images F18_(2010-2013) and F16_2009 that required correction, exhibited poor regression. Consequently, corrected F16_2006 was selected as the reference for images F16_2009 and F18_(2010-2013) (Cao, 2015). The images still could not be directly compared despite saturation correction. Therefore, the mutual correction was performed utilizing the linear mutual correction coefficients between radiometrically calibrated image F16_2006 and other radiometrically calibrated images from the NGDC website (Letu et al., 2012) (Table 2).

$$DN_{ri0}=a_0\times DN_{iac0}^2+b_0\times DN_{iac0}+c_0 \quad (1)$$

where and are the DN of pixels in the corrected and to-be-corrected images, respectively; α0, b0, and

c0 are the parameters of the quadratic polynomial.

$$DN_{ri1}=a_1\times DN_{iac1}+c_1 \quad (2)$$

where DNri1 and DNiαc1 are the DN of pixels in the corrected and to-be-corrected images, respectively; a1 and c1 are the parameters of the linear model.

Table 1. Reference Image Corresponding to the Images to Be Corrected

Radiometrically calibrated light image	Image to be corrected
F12_1996	F10 (1992-1994), F12 (1994-1999)
F12-F15_2000	F14 (1997-2003)
F14-F15_2002	F15 (2000-2007)
F16_2006	F16 (2004-2008)
Corrected F16_2006	F16_2009, F18 (2010-2013)

Table 2. Mutual Correction Coefficients between Radiometrically Calibrated Images

Radiometrically calibrated light image	a_1	c_1	R^2
F12_1996	4.336	0.915	0.971
F12_1999	1.423	0.78	0.98
F12-F15_2000	3.658	0.71	0.98
F14-F15_2002	3.736	0.797	0.98
F14_2004	1.062	0.761	0.984
F16_2006	0	1	1
F16_2010	2.196	1.195	0.981
F16_2010-2011	-1.987	1.246	0.981

Intra-year fusion correction. Images from different sensors may overlap within the same year. These overlapping images are standardized to achieve intra-year fusion, which mitigates the impacts of multiple sensors.

Continuity correction. Theoretically, the pixel values of nighttime light images should either increase or remain constant compared to the previous year. Therefore, continuous DMSP/OLS nighttime light images can be obtained through continuity correction.

$$DN_{(t,i)}=\begin{cases}\&0 & DN_{(t+1,i)}<0\\ \&DN_{(t-1,i)} & DN_{(t+1,i)}>0 \,//\, DN_{(t-1,i)}>DN_{(t,i)}\\ \&DN_{(t,i)} & others\end{cases} \quad (3)$$

where DN (t-1, i), DN (t, i), and DN (t+1, i) are the DN of the i pixel in the image after the first two correction steps for the (t-1), t, and (t+1) year, respectively.

NPP/VIIRS nighttime light images were provided as monthly data. The average of these monthly images was calculated for each year to generate the corresponding annual images.

Outlier Handling. NPP/VIIRS data might contain background noise and outliers (negative and maximum values) due to the sensor's high sensitivity to light sources. Consequently, outlier processing and denoising were necessary. Initially, negative values were set to 0, and the maximum pixel value observed in Guiyang (GY) was designated as the maximum value of the image. Based on officially released 2015 and 2016 annual data, the background values of images in 2012-2015 were standardized using the official images in 2015. Similarly, the background values of images in 2016-2022 were unified with those of official annual images in 2016. Various studies have demonstrated effective methodologies for outlier removal and correction in NPP/VIIRS nighttime light data, ensuring improved data accuracy and consistency (Li, Cao, Zhao, Jie, Liu, Chen, & Cui, 2023).

Inter-year correction. The method was identical to the inter-year correction applied to DMSP/OLS nighttime light images. Images undergoing outlier handling in 2012-2022 were subjected to inter-year correction to produce a continuous series of NPP/VIIRS nighttime light images. Previous studies have demonstrated that inter-calibration between DMSP/OLS and NPP/VIIRS data improves temporal consistency and long-term usability for socioeconomic and urbanization analysis (Bian, Li, Lei, Zhang, Nan, & Liang, 2019; Chen, Yu, Yang, Zhou, Yao, Qian, Wang, Wu, & Wu, 2020). A pixel-scale correction approach has been developed to enhance the spatial and temporal accuracy of such datasets, further supporting their application in long-term studies (Li, Cao, Zhao, Jie, Liu, Chen, & Cui, 2023).

The corrected nighttime light images were comparable. DMSP/OLS and NPP/VIIRS images were combined to create a continuous sequence of nighttime lighting data from 1992 to 2022.

Image fitting. DMSP/OLS nighttime light images were resampled to a resolution of 500 m. Overlapping lighting data in 2012-2013 were extracted for linear, quadratic polynomial, logarithmic, and power regression analyses. GY, the provincial capital of Guizhou, was chosen for brightness analysis due to the province's low-level development. The power function model (Eq. 4) of overlapping images with optimal fit in 2013 was selected. Fitting absolute coefficient R2 = 0.722, which satisfies the required data accuracy.

$$DN_{nh}=16.790\times DN_{iac2}^{0.602} \quad (4)$$

where and are the DN of pixels in images after fitting and to be fitted, respectively; 16.790 and 0.602 are the parameters of the power function model.

Intra-year fusion and inter-year correction. The principle of this method is identical to that of DMSP/OLS nighttime light image correction.

2.2 Methods

2.2.1 Extraction of Urban built-up Areas

The traditional data comparison method allows for a rapid assessment of urban built-up areas. This

method employs bisection iteration to determine the threshold value (Eq. 5) and then calculates the pixel area exceeding this value. If the optimal threshold is identified as the one yielding the highest statistical area accuracy, grid pixels below this threshold are converted into vector patches. The built-up areas of Guizhou for the years 1992, 1995, 2000, 2005, 2010, 2015, 2020, and 2022 are extracted for the calculation and analysis of the expansion index, standard deviation ellipse, and urban spatiotemporal evolution.

$$DN = int\left[(DNmin_{max}\right] \tag{5}$$

where DN is the threshold; DNmax and DNmin are the DN of the maximum and minimum pixels within the half-region during the bisection iteration for the same year, respectively.

2.2.2 Urban Expansion Index

The urban expansion index encompasses the expansion speed and expansion intensity (Eqs. 6-7), which quantifies how quickly urban land grows and the share of increased urban land in the total area of the corresponding unit over a specific period.

$$ER = \frac{s_1 - s_0}{\triangle t} \tag{6}$$

$$EI = \frac{s_1 - s_0}{s_t \times \triangle t} \tag{7}$$

where ER and EI are the expansion speed and intensity, respectively; s0 and s1 are the acreages of built-up areas in the two periods separated by a time interval △t; st is the total area of administrative units.

2.2.3 Standard Deviation Ellipse

Standard deviation ellipse is extensively employed in monitoring built-up areas and the spatiotemporal evolution of urban agglomerations. It visually represents spatial characteristics (e.g., central location, dispersion degree, and direction) as well as the spatial distribution and evolution of cities[40]. Eqs. 7-13 show the calculation process.

Centroid could be defined by

$$(\overline{X}, \overline{Y}) = \left(\frac{\sum_{i=1}^{n} k_i x_i}{\sum_{i=1}^{n} k_i}, \frac{\sum_{i=1}^{n} k_i y_i}{\sum_{i=1}^{n} k_i}\right) \tag{8}$$

where (xi, yi) is the coordinates of the ith built-up area patch; ki is the spatial weight of the patch.

Rotation angle θ is defined by

$$tan\,\theta = \frac{A + \sqrt{A^2 + B^2}}{B} \tag{9}$$

$$A = \sum_{i=1}^{n} (x_i - \overline{X})^2 - \sum_{i=1}^{n} (y_i - \overline{Y})^2 \tag{10}$$

$$B = 2\sum_{i=1}^{n} (x_i - \overline{X})(y_i - \overline{Y}) \tag{11}$$

Standard deviations of x- and y-axes are defined by

$$\sigma_X = \sqrt{2}\sqrt{\frac{\sum_{i=1}^{n} \left[(x_i - \overline{X})\cos\theta - (y_i - \overline{Y})\sin\theta\right]2}{n}} \tag{12}$$

$$\sigma_y = \sqrt{2}\sqrt{\frac{\sum_{i=1}^{n} \left[(x_i - \overline{X})\sin\theta - (y_i - \overline{Y})\cos\theta\right]2}{n}} \tag{13}$$

2.2.4 Kernel Density Estimation

Kernel density estimation, a geospatial analysis technique, was utilized to calculate the density of features within their proximity. The density distribution across the entire research area was determined by overlaying the density surface of all feature points. The correlation between nighttime lighting intensity in built-up areas and the surrounding kernel density was computed to investigate urban clustering characteristics and identify the core development zone in Guizhou.

$$f(x)=\frac{1}{n\times r}\sum_{i=1}^{n}k(\frac{Dij}{r}) \tag{14}$$

where is the kernel density of any point x in the space; is the kernel function; r is the search radius (bandwidth); Dij is the distance weight from point j to center point i within radius r; n is the number of points within radius r.

Pixels with values exceeding the optimal threshold for identifying built-up areas were transformed into points. The DN of the pixels at the location of each point was utilized as the attribute value. This approach was employed to analyze the spatial aggregation characteristics of urban built-up areas in Guizhou, which facilitated the identification of urban cores.

2.2.5 Hotspot Analysis (Getis-Ord Gi*)

Getis-Ord Gi* was used to identify statistically significant hot and cold spots during urban development.

$$Z(G_i^*)=\frac{\sum_j^n W_{ij}(d)x_j}{\sum_j^n x_j} \tag{15}$$

When the results of is standardized,

$$Z(G_i^*)=\frac{\left[G_i^*-E(G)\right]}{\sqrt{Var(G_i^*)}} \tag{16}$$

where is the connection matrix between cities *i* and *j*; x_i and x_j are the growth areas of built-up areas in cities *i* and *j*, respectively; *E (G)* and are the mathematical expectation and variation coefficient of G_i^*, respectively. A high and significant *z* score for a feature indicates that there is high-value spatial clustering as a hotspot. A low and significantly negative *z* score suggests that there is low-value spatial clustering as a cold spot. The higher (or lower) the *z* score corresponds to a greater clustering degree. A *z* score close to zero implies no significant spatial clustering.

3. Results

3.1 Temporal Characteristics of Urban Expansion

The model parameters for quadratic regression in 1992-2013 were derived after DMSP/OLS data underwent saturation correction, mutual correction, intra-year fusion, and continuity correction. These refined model parameters demonstrated a high level of accuracy, with an average correlation coefficient of 0.89. The model was well-fitted to the power function of corrected NPP/VIIRS data, with a

correlation coefficient of 0.72 for the fit (Table 3). Fig. 2 illustrates nighttime lighting data from 1992 to 2022 (a and b represent the images before and after correction, respectively).

Table 3. Parameters of DMSP/OLS and NPP/VIIRS Image Correction

image	a_0	b_0	c_0	R^2	image	a	b	c	R^2
F10_1992	0.337	0.028	4.476	0.870	F15_2001	0.520	0.077	9.423	0.865
F10_1993	0.608	0.033	2.182	0.932	F15_2002	1.390	0.084	14.956	0.929
F10_1994	0.565	0.029	2.587	0.957	F15_2003	0.544	0.080	10.113	0.911
F12_1994	0.617	0.023	2.432	0.924	F15_2004	1.158	0.083	13.140	0.915
F12_1995	0.405	0.025	3.296	0.951	F15_2005	1.043	0.082	12.692	0.815
F12_1996	0.181	0.031	4.848	0.951	F15_2006	1.704	0.096	15.549	0.906
F12_1997	0.479	0.026	2.473	0.945	F15_2007	1.109	0.089	12.523	0.870
F12_1998	0.117	0.027	4.710	0.936	F16_2004	0.322	0.042	7.752	0.831
F12_1999	0.161	0.028	5.308	0.905	F16_2005	0.038	0.045	6.412	0.905
F14_1997	0.417	0.067	4.439	0.944	F16_2006	0.186	0.049	6.675	0.907
F14_1998	0.086	0.068	6.329	0.907	F16_2007	0.444	0.049	8.406	0.892
F14_1999	0.135	0.066	5.928	0.927	F16_2008	0.645	0.050	9.304	0.829
F14_2000	0.646	0.065	10.077	0.936	F16_2009	1.398	0.058	14.268	0.918
F14_2001	0.652	0.059	10.587	0.913	F18_2010	1.895	0.056	20.416	0.816
F14_2002	0.635	0.051	10.677	0.833	F18_2011	-1.134	0.050	12.806	0.836
F14_2003	1.004	0.057	13.198	0.852	F18_2012	1.709	0.059	17.120	0.900
F15_2000	0.846	0.081	11.851	0.833	F18_2013	1.765	0.052	18.819	0.764

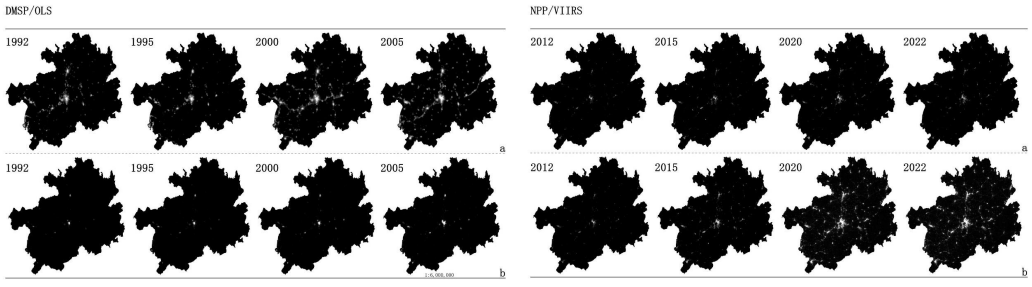

Figure 2. Remotely Sensed Images of Nighttime Light in Guizhou from 1992 to 2022

Urban built-up areas of Guizhou in 1992, 1995, 2000, 2005, 2010, 2015, 2020, and 2022 were identified using the traditional data comparison method based on the processed nighttime light images from 1992 to 2022. These extraction results were compared with built-up areas released by the Guizhou Provincial Bureau of Statistics. The comparison revealed high accuracy in our extraction (Fig. 3), with the maximum absolute error not exceeding 3%. For instance, this accuracy was demonstrated in the case of Zunyi (ZY)(Table 4).

Table 4. Accuracy of Urban Built-up Area in Guizhou Using Nighttime Light Remote Sensing

Year	real area (km^2)	calculated value (km^2)	threshold	relative error (%)	absolute error (km^2)
1992	202.3	196.25	34	2.99	6.05
1995	233.3	231.75	40	0.66	1.55
2000	305.75	303.75	50	0.65	2
2005	706.19	715.75	39	1.35	9.56
2010	972.99	968.75	56	0.44	4.24
2015	1458.83	1479.25	67	1.40	20.42
2020	2010.38	2031.25	81	1.04	20.87
2022	2074.73	2114	82	1.89	39.27

The urban built-up areas in Guizhou consistently grew from 202.3 km² in 1992 to 2,074.73 km² in 2022, a 925% increase. The speed and intensity of urban expansion in Guizhou followed an M-shaped pattern of fluctuations. Initially, urban development was slow in 1992-2000. The first phase of rapid growth occurred in 2000-2005. This growth rate decreased in 2005-2010 compared to the previous period. A period of sustained rapid development peaked in 2010-2020, and the growth rate declined in 2020-2022.

The speed and intensity of urban expansion significantly vary among Guizhou's prefecture-level cities (Fig. 3), falling into four distinct categories: stable, fluctuating, breakthrough, and gradual. The expansion speed and intensity steadily grow at a high level in the stable category. The fluctuating category exhibits varying speeds and intensities. Expansion steadily accelerates and intensifies in the early stages and suddenly peaks at a specific period in the breakthrough category. The gradual category experiences slow and steady growth of the expansion speed and intensity at a low level.

GY, an example of the stable category, led Guizhou in urban development, reaching a peak expansion speed of 45 km²/year in 2000-2005. Liupanshui (LPS), classified in the fluctuating category,

experienced a pattern of alternating high and low expansion speeds and intensities, with a notable negative growth rate in 2010-2015. ZY, part of the breakthrough category, exhibited an increased expansion speed in 1992-2020. The expansion speed of 31 km2/year in 2015-2020 significantly surpassed that of other prefecture-level cities. Tongren (TR), Bijie (BJ), Anshun (AS), and regions like Southwest, Southeast, and Southern Guizhou fell under the gradual category. They were characterized by initial slow growth and low intensity, which improved in 2010-2020.

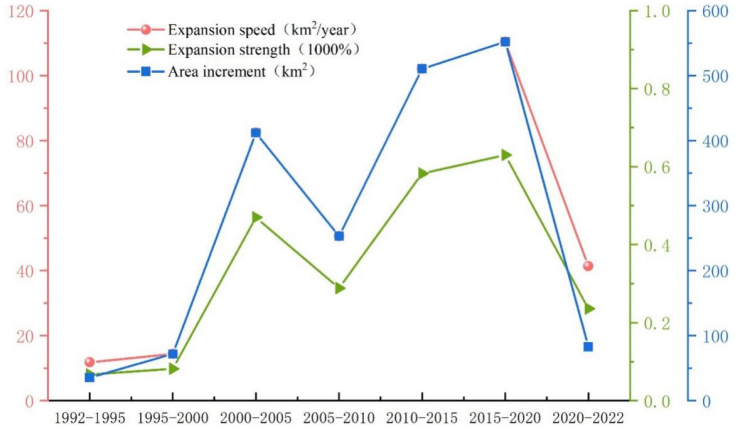

Figure 2. Expansion speed, Expansion Intensity, and Area Growth in Guizhou

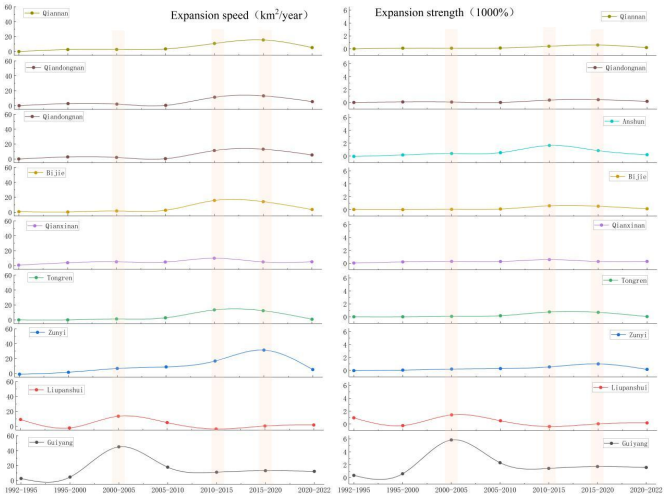

Figure 3. Urban Expansion Speed and Intensity of Prefecture-level Cities in Guizhou during Various Periods

3.2 Urban Expansion Direction and Development Focus Migration

A standard deviation ellipse was created based on the vector patches of built-up areas in 1992, 1995, 2000, 2005, 2010, 2015, 2020, and 2022 (Fig. 5).

The azimuthal angle of the standard deviation ellipse shifted from 42 to 49° and then back to 43°. Overall, urban expansion in Guizhou predominantly occurred along the northeast-southwest axis, with

primary development in the main direction followed by secondary ones. However, two distinct periods deviated from this trend: The major axis was shortened by 12.3 km, while the minor axis slowly lengthened in 2000-2005, which signified a focus on central city development. The major axis extended by 7 m and the minor axis by 1,619 m in 2020-2022, indicating that cities developed towards secondary directions.

The centroid of the standard deviation ellipse, indicative of the focal point of urban development, shifted 42.03 km northeast in the direction of ZY in the past 30 years. The most significant migration occurred in GY from 2015-2020, moving 23.36 km to the northeast. Initially, the development focus was on the convergence of GY, BJ, and AS Cities in 1992-2005. Since then, it has been centered in GY, which is the primary hub of development in the region. The development focus shifted 21.89 km southwest from GY to BJ in 1992-2000, which highlighted the significant role of southwestern cities in Guizhou's urban development. Subsequently, it moved another 21.39 km southwest from BJ to AS and gradually inched back towards the central region. The focus shifted northeast in 2000-2020 and reached GY in 2010, indicative of the emerging importance of northeastern cities. The central urban area remained stable in 2020-2022, while southeastern cities transitioned into a later stage of development.

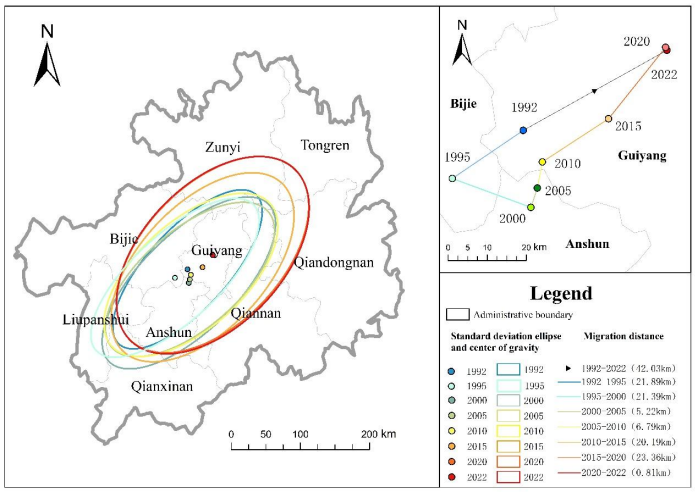

Figure 5. Standard Deviation Ellipse of Built-up areas in Guizhou and Migration of Urban Development Focus

3.3 Distribution and Evolution of Urban cores in Guizhou

The values were divided into 5 categories using the thresholds of 6.01, 27.02, 69.06, and 146.13 to facilitate comparison across different stages and elucidate patterns. The categorization was derived from the natural breakpoint method for Kernal density in Guizhou in 2020. Categories 1 and 2 represented low-value areas, followed by the micro core, secondary core, and main core.

The urban core of Guizhou evolved through distinct phases from 1992 to 2022. Initially, GY was the sole micro core and then evolved into the main core. Ultimately, a hierarchical urban structure took

shape, with GY as the main core, ZY as a secondary core, and a constellation of Kaili, Duyun, and Fuquan Cities as peripheral micro cores. This system was characterized by GY's influence on AS and the decentralized growth of other cities (Fig. 6).

GY was the sole micro core of urban development in Guizhou from 1992-2000 due to the province's low urbanization level. An urban structure emerged by 2005, with GY as the main core area and ZY as a micro core area. GY remained the main core area in 2010, while ZY's micro core area expanded. Besides, micro cores appeared in LPS and Southwest Guizhou. Every core area experienced growth in 2015, with AS exhibiting new cores. ZY evolved into a secondary core area in 2020, and Southwest Guizhou showed the potential to become a secondary core area. GY and AS Cities developed in tandem. TR, Southeast Guizhou, and Southern Guizhou exhibited micro cores. Guizhou's urban structure displayed minimal changes by 2022, which reflected the slow pace of urban development.

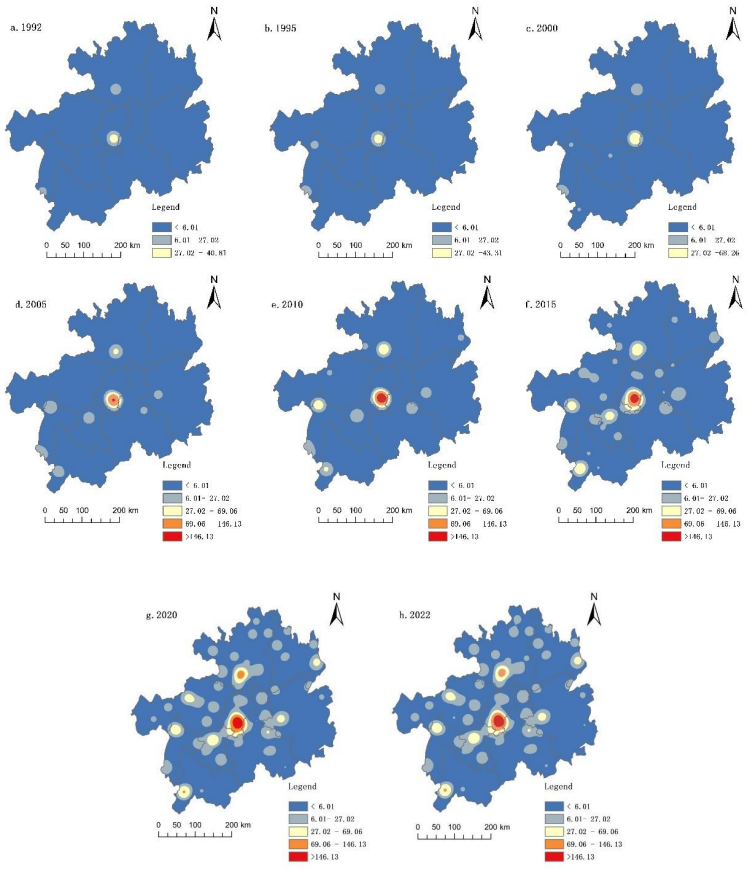

Figure 6 Kernal Density of Urban Expansion in Guizhou from 1992 to 2022

County territories, fundamental to China's economic growth, are important in accommodating urban expansion. The work employed 88 county units in Guizhou to calculate the Getis-Ord Gi* index of urban expansion for built-up areas across different time frames. This approach enabled the identification of hot and cold spots during urban development (Kowe, Dube, Mushore, Ncube, Nyenda,

Mutowo, Chinembiri, Traore, & Kizilirmak, 2022). The Z-scores were categorized into five grades using the natural breakpoint method (Chen, Wang, Xiong, Sun, & Xu, 2022) (Fig. 7).

Hot and cold spots of urban development in Guizhou underwent marked changes from 1992 to 2022, with significant differentiation. GY exerted radiating influence on adjacent districts and counties, particularly Longli County. The city remained a stable hotspot area, with most of its districts and counties exhibiting hotspots for three decades. LPS and the southern districts of Southwest Guizhou emerged as hotspot areas for urban expansion in 1992-2000. Subsequently, these areas transitioned to sub-cold spot areas as expansion slowed, while some districts and counties evolved into sub-hot spot areas. ZY, previously a cold spot area, became a hotspot area for development from 2015 to 2020. However, it reverted to a cold spot area in 2022.

AS and the districts and counties in Southern Guizhou near GY emerged as hotspot areas under the radiating influence of GY. Driven by GY, northern cities experienced a brief period as hotspot areas from 2010-2015, while western and southern cities remained as cold and sub-cold spot areas. BJ predominantly remained as cold and sub-cold spot areas. However, spurred by the growth of GY and ZY Cities, sub-hot spots occurred in BJ during two distinct periods in 2010-2020, respectively. TR, Southeast Guizhou, and southern districts and counties in Southern Guizhou remained as cold and sub-cold spot areas for an extended period.

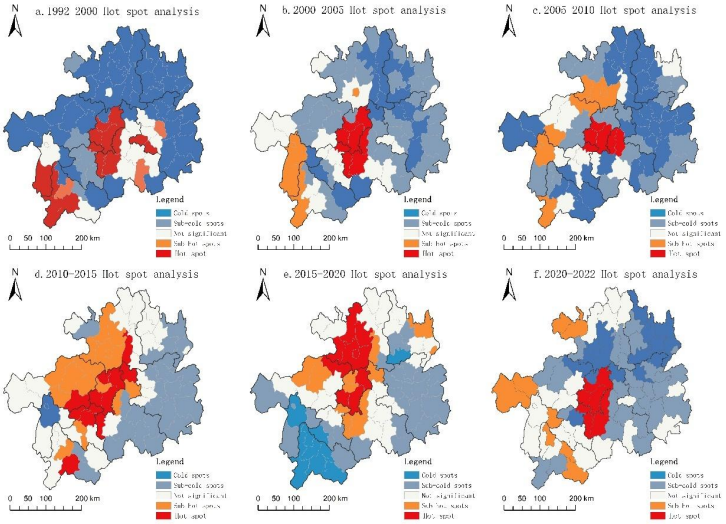

Figure 7. Cold and Hot Spot Distribution of Development Spaces in Guizhou from 1992 to 2022

4. Discussions

Guizhou's urban expansion over the past three decades has been remarkable, increasing from 202.3 km² in 1992 to 2,074.73 km² in 2022, a staggering 925% growth. This expansion exhibited an M-shaped fluctuation pattern, with rapid phases occurring between 2000–2005 and 2010–2020. The study categorized urban expansion in prefecture-level cities into four types—stable, fluctuating, breakthrough, and gradual—and identified three major expansion models: ring-like, linear (axis), and punctate. The

overall development track followed a northeast-southwest axis, with the focus shifting from GY northeastward before returning in 2010 and moving southeastward after 2020. The spatial pattern of urbanization evolved into a hierarchical structure, with GY as the main core, ZY as a secondary core, and a cluster of smaller cities forming peripheral micro cores. Hotspot analysis revealed stable central urban hotspots, emerging hotspots in ZY, and projected future development in southeastern and southern Guizhou.

This study highlights the potential of long-term nighttime light remote sensing for analyzing urban expansion in mountainous areas, employing metrics such as expansion speed, intensity, standard deviation ellipse, kernel density, and hotspot analysis. However, challenges persist, including topographic effects that obscure nighttime lights and atmospheric scattering that may affect data accuracy. Future studies must refine remotely sensed image processing algorithms and integrate multi-source remote sensing to enhance precision. Despite these challenges, nighttime light remote sensing offers a unique perspective on mountainous urban development, with significant applications in urban expansion monitoring, socio-economic assessment, and environmental impact analysis. Advancing image fusion and model optimization will be key to supporting the sustainable development of mountainous cities.

References

Ouyang, Z., Lin, M., Chen, J., Fan, P., Qian, S., & Park, H. (2019). Improving estimates of built-up area from nighttime light across globally distributed cities through hierarchical modeling. *Science of the Total Environment*, *647*, 1266-1280.

He, X., Li, Z., Guo, H., Tian, Z., & Wang, X. (2019). Analyzing the consistency between built-up areas and human activities and the impacts on the urbanization process: A case study of Zhengzhou, China. *International Journal of Remote Sensing*, 40(15), 6008-6035.

Zheng, Q., Seto, K. C., Zhou, Y., et al. (2023). Nighttime light remote sensing for urban applications: Progress, challenges, and prospects. *ISPRS Journal of Photogrammetry and Remote Sensing*, *202*, 125-141.

Zheng, Z., Wu, Z., & Qian, Q. (2019). *Review and prospect of application of nighttime light remote sensing data*, *38*(2), 205-223.

Levin, N., & Duke, Y. (2012). High spatial resolution nighttime light images for demographic and socio-economic studies. *Remote Sensing of Environment*, *119*, 1-10.

Zhao, M., Zhou, Y., Li, X., Cao, W., He, C., Yu, B., Li, X., Elvidge, C., Cheng, W., & Zhou, C. (2019). Applications of satellite remote sensing of nighttime light observations: Advances, challenges, and perspectives. *Remote Sensing*, *11*, 1971.

Levin, N., Kyba, C. C. M., Zhang, Q., et al. (2020). Remote sensing of night lights: A review and an outlook for the future. *Remote Sensing of Environment*, *237*, 111443.

Huang, T., Luo, J., Wang, Y., & Huang, F. (2021). Urban expansion analysis of GBA based on

multi-source nighttime light remote sensing images. *2021 Photonics & Electromagnetics Research Symposium (PIERS)*, 1952-1960.

Hu, X., Qian, Y., Pickett, S. T. A. et al. (2020). Urban mapping needs up-to-date approaches to provide diverse perspectives of current urbanization: A novel attempt to map urban areas with nighttime light data. *Landscape and Urban Planning*, *195*, 103709.

Ma, X., Li, C., Tong, X., & Liu, S. (2019). A new fusion approach for extracting urban built-up areas from multisource remotely sensed data. *Remote Sensing*, *11*, 2516.

Xie, Y., Weng, Q., & Weng, A. (2014). A comparative study of NPP-VIIRS and DMSP-OLS nighttime light imagery for derivation of urban demographic metrics. *2014 Third International Workshop on Earth Observation and Remote Sensing Applications (EORSA)*, 335-339.

Amaral, S., Monteiro, A. M. V., Câmara, G. et al. (2006). DMSP/OLS nighttime light imagery for urban population estimates in the Brazilian Amazon. *International Journal of Remote Sensing*, *27*(5), 855-870.

Ou, J., Liu, X., Li, X., & Li, M. (2015). Evaluation of NPP-VIIRS nighttime light data for mapping global fossil fuel combustion CO_2 emissions: A comparison with DMSP-OLS nighttime light data. *PLOS ONE*, *10*(9), e0138310.

Hillger, D., Seaman, C., Liang, C. et al. (2014). Suomi NPP VIIRS imagery evaluation. *Journal of Geophysical Research: Atmospheres*, *119*(11), 6440-6455.

Bian, J., Li, A., Lei, G., Zhang, Z., Nan, X., & Liang, L. (2019). Inter-calibration of nighttime light data between DMSP/OLS and NPP/VIIRS in the economic corridors of Belt and Road Initiative. *IGARSS 2019-2019 IEEE International Geoscience and Remote Sensing Symposium,* 9028-9031.

Chen, Z., Yu, B., Yang, C., Zhou, Y., Yao, S., Qian, X., Wang, C., Wu, B., & Wu, J. (2021). An extended time series (2000–2018) of global NPP-VIIRS-like nighttime light data from a cross-sensor calibration. *Earth System Science Data*, *13*, 889-906.

Ma, T., Zhou, Y., Zhou, C., et al. (2015). Nighttime light-derived estimation of spatio-temporal characteristics of urbanization dynamics using DMSP/OLS satellite data. *Remote Sensing of Environment*, *158*, 453-464.

Zhao, M., Zhou, Y., Li, X., Zhou, C., Cheng, W., Li, M., & Huang, K. (2020). Building a series of consistent nighttime light data (1992-2018) in Southeast Asia by integrating DMSP-OLS and NPP-VIIRS. *IEEE Transactions on Geoscience and Remote Sensing*, *58*, 1843-1856.

Yongzhen, L., Byambakhuu, G., Battsengel, V., Sainbuyan, B., & Altanbold, E. (2022). Applicability analysis of nighttime lights data in the development research using DMSP/OLS and NPP/VIIRS satellite imagery: An example in Mongolia. *Geographical Issues*, *22*(02), 93-103.

Li, S., Cao, X., Zhao, C., Jie, N., Liu, L., Chen, X., & Cui, X. (2023). Developing a pixel-scale corrected nighttime light dataset (PCNL, 1992-2021) combining DMSP-OLS and NPP-VIIRS. *Remote Sensing*, *15*(16), 3925.

Huang, Y., Yang, J., Chen, M., Wu, C., Ren, H., & Liu, Y. (2022). An approach for retrieving consistent

time series “Urban Core-Suburban-Rural” (USR) structure using nighttime light data from DMSP/OLS and NPP/VIIRS. *Remote Sensing*, *14*, 3642.

Zhang, M., He, Z., & Fan, Y. (2017). Calibration for DMSP/OLS stable nighttime light images. *Bulletin of Surveying and Mapping*, *58*.

Wang, Z., Zheng, J., Han, C. et al. (2025). A comprehensive assessment approach for multiscale regional economic development: Fusion modeling of nighttime lights and OpenStreet Map data. *Geography and Sustainability*, *6*(2), 100230.

Ju, Y., Dronova, I., Ma, Q., et al. (2017). Analysis of urbanization dynamics in mainland China using pixel-based nighttime light trajectories from 1992 to 2013. *International Journal of Remote Sensing*, *38*(21), 6047-6072.

Tan, M. (2015). Urban growth and rural transition in China based on DMSP/OLS nighttime light data. *Sustainability*, *7*, 8768-8784.

Zheng, Y., Tang, L., & Wang, H. (2021). An improved approach for monitoring urban built-up areas by combining NPP-VIIRS nighttime light, NDVI, NDWI, and NDBI. *Journal of Cleaner Production*, *328*, 129488.

Wu, J., Tu, Y., Chen, Z. et al. (2022). Analyzing the spatially heterogeneous relationships between nighttime light intensity and human activities across Chongqing, China. *Remote Sensing*, *14*(22), 5695.

Jia, L., Ma, Q., Du, C. et al. (2020). Rapid urbanization in a mountainous landscape: Patterns, drivers, and planning implications. *Landscape Ecology*, *35*, 2449-2469.

Chen, G., Zhou, Y., Voogt, J. A. et al. (2024). Remote sensing of diverse urban environments: From the single city to multiple cities. *Remote Sensing of Environment*, *305*, 114108.

Song, Y., Li, X., Tao, G., & Liu, J. (2023). Exploring the characteristics and drivers of expansion in the Shandong Peninsula urban agglomeration based on nighttime light data. *IEEE Journal of Selected Topics in Applied Earth Observations and Remote Sensing*, *16*, 8535-8549.

Wu, K., & Wang, X. (2019). Aligning pixel values of DMSP and VIIRS nighttime light images to evaluate urban dynamics. *Remote Sensing*, *11*, 1463.

Shen, Z., Zhu, X., Cao, X., & Chen, J. (2019). Measurement of blooming effect of DMSP-OLS nighttime light data based on NPP-VIIRS data. *Annals of GIS*, *25*, 153-165.

Zhang, M., He, Z., & Fan, Y. (2017). Calibration for DMSP/OLS stable nighttime light images. *Bulletin of Surveying and Mapping*, *58*.

Wu, J., He, S., Peng, J., Li, W., & Zhong, X. (2013). Intercalibration of DMSP-OLS nighttime light data by the invariant region method. *International Journal of Remote Sensing*, *34*, 7356-7368.

Hu, Y., Chen, J., Cao, X., Chen, X., Cui, X., & Gan, L. (2021). Correcting the saturation effect in DMSP/OLS stable nighttime light products based on radiance-calibrated data. *IEEE Transactions on Geoscience and Remote Sensing*, *60*, 1-11.

Wang, Z., Yao, F., Li, W., & Wu, J. (2017). Saturation correction for nighttime lights data based on the

relative NDVI. *Remote Sensing*, *9*, 759.

Cao, Z. (2015). Correction of DMSP/OLS nighttime light images and its application in China. *Journal of Geo-information Science*.

Letu, H., Hara, M., Tana, G., & Nishio, F. (2012). A saturated light correction method for DMSP/OLS nighttime satellite imagery. *IEEE Transactions on Geoscience and Remote Sensing*, *50*, 389-396.

Chen, Z., Yu, B., Yang, C., Zhou, Y., Yao, S., Qian, X., Wang, C., Wu, B., & Wu, J. (2020). An extended time series (2000-2018) of global NPP-VIIRS-like nighttime light data from a cross-sensor calibration. *Earth System Science Data*, *13*, 889-906.

Song, Y., Gui, Z., Wu, H., & Wei, Y. (2017). A web-based framework for visualizing industrial spatiotemporal distribution using standard deviational ellipse and shifting routes of gravity centers. *ISPRS - International Archives of the Photogrammetry, Remote Sensing and Spatial Information Sciences*, *42*(2/W7), 129-135.

Kowe, P., Dube, T., Mushore, T., Ncube, A., Nyenda, T., Mutowo, G., Chinembiri, T. S., Traore, M., & Kizilirmak, G. (2022). Impacts of the spatial configuration of built-up areas and urban vegetation on land surface temperature using spectral and local spatial autocorrelation indices. *Remote Sensing Letters*, *13*, 1222-1235.

Chen, Y., Wang, J., Xiong, N., Sun, L., & Xu, J. (2022). Impacts of land use changes on net primary productivity in urban agglomerations under multi-scenarios simulation. *Remote Sensing*, *14*, 1755.